Journal of Applied Fluid Mechanics, Vol. 9, No. 5, pp. 2537-2544, 2016.
Available online at www.jafmonline.net, ISSN 1735-3572, EISSN 1735-3645.
DOI: 10.18869/acadpub.jafm.68.236.25136

2-D Urans Simulations of Vortex Induced Vibrations of Circular Cylinder at Trsl3 Flow Regime

O. K. Kinaci

Naval Architecture and Maritime Faculty, Yildiz Technical University, Istanbul-34349, Turkey

Email: kinaci@yildiz.edu.tr

(Received June 4, 2015; accepted September 8, 2015)

ABSTRACT

Research on vortex-induced vibrations (VIV) mainly involves experimental science but building laboratory setups to investigate the flow are expensive and time consuming. Computational fluid dynamics (CFD) methods may offer a faster and a cheaper way to understand this phenomenon depending on the solution approach to the problem. The context of this paper is to present the author's computational approach to solve for vortex-induced vibrations which cover extensive explanations on the mathematical background, the grid structure and the turbulence models implemented. Current computational research on VIV for smooth cylinders is currently restricted to flows that have Reynolds numbers below 10,000. This paper describes the method to approach the problem with URANS and achieves to return satisfactory results for higher Reynolds numbers.The computational approach is first validated with a benchmark experimental study for rather low Reynolds number which falls into TrSL2 flow regime. Then, some numerical results up to $Re = 130{,}000$, which falls into TrSL3 flow regime,are given at the end of the paper to reveal the validity of the approach for even higher Reynolds numbers.

Keywords: Vortex-induced vibrations; Fluid-induced motions; Computational fluid dynamics; URANS.

NOMENCLATURE

a	acceleration of the cylinder	k	spring stiffness
A	amplitude	m	oscillating mass
c	mechanical damping	m_a	added mass
D	diameter of the cylinder	t	time step
$f_{n,a}$	natural frequency in air	U	velocity of the cylinder
$f_{n,w}$	natural frequency in water	U_{fs}	free-stream velocity of the fluid
f^*	non-dimensional frequency	U^*	reduced velocity
F	fluid force	y	displacement

1. INTRODUCTION

Flow-induced motions have attracted attention in the last 50 years, mainlyafter the offshore industry has increased their investments in oceans. The large amplitude vibrations of tethered structures in the oceans cause structural problems. These motions are also encountered in many other engineering fields and these are explained thoroughly in review papers of (Sarpkaya, 2004)and(Willimson & Govardhan, 2004).

Vortex-induced vibration is a form of fluid-induced motions and is a phenomenon that every form of matter may get affected that is subjected to a fluid flow. Vortex-induced vibrations are highly nonlinear and this nonlinearity of the flow increases the complexity of the computations. Before powerful computers have emerged to serve the academic research in this field, the early research on vortex-induced vibrations was mostly focused on experimental science. However, the rapid technological progress in computer science has increased the capability of approaching the problem computationally in the last 20 years. Despite these improvements in computers, mathematical approaches to solve for vortex-induced vibrations still involve high computational demands. The

difficulty in solving the flow urges the researchers of this field to make many assumptions and there are many ways to approach vortex-induced vibration problems computationally. The scope of this study is limited to the vortex-induced-vibrations of rigid circular cylinders on elastic supports. The cylinder is restricted to oscillate transversely to the fluid flow. Due to two-dimensional approach implemented in this study, the effects of tip flow are neglected. Two-dimensional flow assumption allows fast computations and gives quantitative notion about the dynamics of the flow.

Current research in the field is limited to flows that are $Re < 10{,}000$ and some works from the literature are briefly mentioned in the following sections. This paper focuses on a thorough URANS application of the problem for flows that are $Re \geq 10{,}000$ for smooth cylinders. The mathematical background, the implemented grid structure, the boundary conditions, the selection of turbulence model and the calculation of time step size are explained in detail and some numerical results validated with experiments are given. After validation of the approach, some numerical results for TrSL3 flow regime ($35{,}000 < Re < 130{,}000$) is presented at the end of the paper.

2. MATHEMATICAL APPROACH

The vibration equation of a cylinder attached with springs subjected to a steady fluid flow is given as;

$$m\ddot{y} + c\dot{y} + ky = F \tag{1}$$

This is the forced oscillation equation. The left hand side deals with the vibration while the right hand side deals with the force applied to the cylinder by the fluid.

Leaving the acceleration term $\ddot{y}$ alone, Eq. (1) becomes;

$$\ddot{y} = \frac{F - c\dot{y} - ky}{m} \tag{2}$$

When the acceleration of the cylinder is known, its velocity and displacement can be calculated by;

$$\int dy = \int \dot{y}\, dt = \iint \ddot{y}\, dtdt \tag{3}$$

Rewriting Eq. (3) in a numerical sense;

$$y_{t+1} = y_t + U_{t+1} \cdot \Delta t \tag{4}$$

$$U_{t+1} = U_t + a_{t+1} \cdot \Delta t \tag{5}$$

The displacement of the cylinder in VIV can therefore be given as;

$$y_{t+1} = y_t + U_t \Delta t + a_{t+1} \cdot (\Delta t)^2 \tag{6}$$

a_{t+1}in Eq. (6) is calculated from Eq. (2). So writing it in numerical form;

$$a_{t+1} = a_t + \frac{F_{t+1} - cU_t - ky_t}{m} \tag{7}$$

Returning back to Eq. (6) and rewriting the numerical displacement equation will read;

$$y_{t+1} = y_t + U_t \Delta t + (a_t + \frac{F_{t+1} - cU_t - ky_t}{m}) \cdot (\Delta t)^2 \tag{8}$$

Eq. (8) gives the displacement of the cylinder at each time step. The force F, applied by the fluid will commence the oscillatory movement of the cylinder. The cylinder is assumed to be at the origin ($y = 0$) and stable at $t = 0$. The initial conditions in mathematical terms are;

$$y_0 = U_0 = a_0 = 0 \tag{9}$$

Just after the flow starts, the displacement of the cylinder will therefore be;

$$y_1 = y_0 + U_0 \Delta t + \left(a_0 + \frac{F_1 - cU_0 - ky_0}{m}\right) \cdot (\Delta t)^2 = \left(\frac{F_1}{m}\right) \cdot (\Delta t)^2 \tag{10}$$

VIV involves a two-way fluid structure interaction (FSI) problem. At each time step, the flow around the cylinder is solved to find the vertical lift force acting on it *as if it is not moving*. This force is then used to find the new displacement at the next time step. This is the first part of the FSI. As the cylinder moves, it also moves the fluid nearby. Therefore, the flow also gets affected by the cylinder's movement. This is the second part of the FSI. So the cylinder gets excited by the fluid and in return, the flow is affected by the cylinder's movement. This will alter the applied fluid force but it must be indicated here that the change in this force F is not visible in Eq. (8). $F$is completely solved by the Navier-Stokes Equations and it is used to find the new displacement in Eq. (8). To identify how the fluid force F is affected by the movement of the cylinder, the Navier-Stokes Equations have to be written down.

The pressure distribution along the cylinder can be calculated from the Navier-Stokes Equations and in two-dimensional form they are given as;

$$\frac{\partial p}{\partial x} = \mu\left(\frac{\partial^2 u}{\partial x^2} + \frac{\partial^2 u}{\partial y^2}\right) - \rho\left(\frac{\partial u}{\partial t} + u\frac{\partial u}{\partial x} + v\frac{\partial u}{\partial y}\right) \tag{11}$$

$$\frac{\partial p}{\partial y} = \mu\left(\frac{\partial^2 v}{\partial x^2} + \frac{\partial^2 v}{\partial y^2}\right) - \rho\left(\frac{\partial v}{\partial t} + u\frac{\partial v}{\partial x} + v\frac{\partial v}{\partial y}\right) \tag{12}$$

Here, x and y denote the Cartesian coordinate system axes. When the cylinder moves in a direction, the horizontal and vertical velocities u and v in the fluid domain also change. This results in a different pressure distribution and so a different fluid force F on the cylinder. The cylinder has one degree-of-freedom and therefore in this work, the vertical lift force F is calculated by;

3. ESTABLISHING THE GRID

The numerical solution to VIV in this paper is based on Finite Volume Method (FVM). The domain needs to be discretized carefully and there are some issues that must be taken into consideration before moving on to solve the flow. There are of course many ways to approach this problem. The current work reveals the author's approach. The points that

need special attention are mentioned in this section of the paper.

3.1. Fluid Zones

Depending on the dynamic mesh method considered to be deployed to move the cylinder, the fluid zones are identified. To obtain accurate results and good vorticity contours, the fluid domain is divided into two. One of them is the dynamic zone and the other one is the static zone. The dynamic zone is formed of two regions which are the near-cylinder region and the wake region. The static zone is only comprised of the outer region. The positions of these regions can be seen in Fig. 1. The dimensions of these zones are identified in the next paragraph.

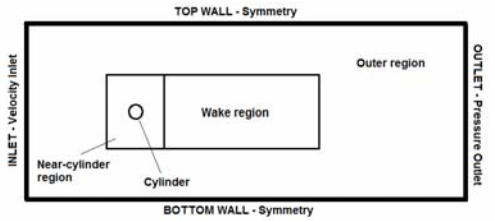

Fig. 1. The fluid domain.

The elements in the dynamic zone are non-deforming because the elements may be deformed heavily around the cylinder which would blow up the numerical simulations. Due to this reason, the cylinder is surrounded by a rectangular near-cylinder region of dimensions $5D * 6D$. The centers of the cylinder and the near-cylinder region are coincident. To capture the wake region correctly and to minimize the possible effects of bad mesh quality on the cylinder, there is a wake region in the fluid domain attached next to the near-cylinder region of dimensions $12D * 6D$. These two regions prevent the numerical simulations to diverge due to poor grid quality and increase the stability and robustness of the results.

3.2. Setting the Boundaries

The domain boundaries are selected far away from the cylinder so that they do not have any effect on the cylinder and the wake. The inlet and outlet boundariesare set to be$10 * D$ and$25 * D$ from the cylinder respectively to minimize boundary impacts on the oscillation. The positions of top and bottom walls should be selected carefully so that when the cylinder oscillates, it does not get very close to the walls.The top and bottom walls are $10 * D$ away from the cylinder. If the cylinder gets close to the walls, this may have two consequences. The first one is; due to the symmetry condition, the cylinder will get affected by the boundary. The second consequence is; due to the re-meshing of cells, the newly formed grids may be corrupted.Considering that the maximum oscillation of the cylinder would be around $2 * D$, the selected top and bottom wall distances are far enough to have any impact on VIV of the cylinder.

The boundaries of the regions are determined so that a better mesh structure could be provided. Using structured grids close to the cylinder and its wake will produce more accurate results and generate better contours.

3.3. y^+ Criterion

The implemented turbulence models usually have a range of y^+ that they work best (ANSYS Fluent 12 User's Guide, 2009). The expanded form of the y^+ formula is given as;

$$y^+ = \frac{\rho y \sqrt{\frac{\mu}{\rho}\left(\frac{\partial u}{\partial y}\right)_{y=0}}}{\mu} \tag{13}$$

Depending on the selected turbulence model, the mesh elements around the cylinder should be imposed accordingly. Please see Section 6 for the selection of turbulence model.

3.4. Grid Type

To obtain better results, structured grid in the near-cylinder and wake regions is implemented. Quadrilateral elements are used in this dynamic fluid zone and for the outer zone, triangular elements are preferred. Near-cylinder region is meshed with an O-grid type of meshing. It is possible that different dynamic mesh methods use different grid types. While meshing the whole domain, demands of the dynamic mesh method that will be implemented to move the cylinder should also be paid regard. The grid in the whole fluid domain and a close-up view in the near-cylinder region are provided in Fig. 2.

4. SETTING THE BOUNDARY CONDITIONS

The boundary conditions are given in Fig. 1. The *velocity inlet* boundary condition is selected for the inlet because it allows imposing the fluid velocity directly. This way it is easier to do simulations at each reduced velocity, U^*. The turbulence parameters at the inlet and the outlet should be imposed on the solver according to the tunnel that is simulated.

The top and bottom walls of the fluid domain are selected to have *symmetry* condition in this study. The selection of the boundary condition type is open to discussion depending on what is to be simulated computationally. An exact simulation of a tunnel needs to have a free surface that separates the air and water phases and a *wall* bottom boundary. However in this study, possible effects of the bottom boundary on the cylinder were to be avoided. If the top and the bottom of the fluid domain were selected to be *walls*, then, the flow close to them would have a boundary layer which might have some effect on the cylinder if it would achieve high amplitudes. The effect of the bottom boundary on VIV is experimentally investigated by (Raghavan, Bernitsas, & Maroulis, 2009).

5. THE DYNAMIC MESH

The grid that is implemented to computationally

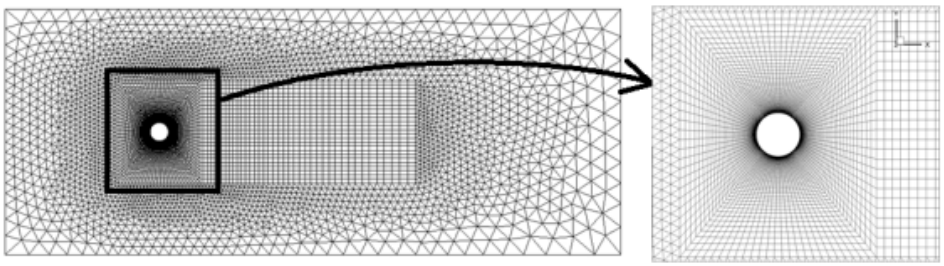

Fig. 2. The mesh structure in the fluid domain.

approach the oscillating cylinder problem is (as explained in Section 3), composed of two zones which are the dynamic zone and the static zone. The dynamic zone, which is the composition of the near-cylinder and wake regions, is allowed to move in the vertical direction but the mesh is not deforming.The static zone, which is the outer region (or in other words, the rest of the fluid domain), is fixed and not moving; however, the mesh is allowed to deform.

Due to constant remeshing of the grid, this authorization of deformation of the static zone usually poses a problem but on the other hand, remeshing allows the whole fluid domain to remain flexible to cylinder's movement. The deformed grid should be closely watched against deterioration of the elements and to avoid highly skewed elements which could, in the end, diverge the whole iterative process. Avoidance of highly skewed elements near the cylinder is a major issue and this is why the elements near the cylinder are not allowed to deform.The maximum allowable skewness of grid elements in the static region is set to be 0.7. Increasing this value will allow poor elements to be formed in the static region. On the other hand, decreasing the maximum allowable skewnesss would result in increased number of elements which would slow down the numerical process.

6. SELECTION OF THE TURBULENCE MODEL

The selection of the turbulence model depends on the geometry, the grid and available computational power. Some of the widely used turbulence models available in the literature are briefly explained in this section and their suitability to solving VIV are discussed. The first three models are called URANS (Unsteady Reynolds-Averaged Navier-Stokes) methods and the fourth part discusses two numerical simulations which provide more advanced solutions. In the last part there is a comparison of results implementing different URANS methods from the literature and the present study.

6.1. URANS: The Spalart – Allmaras Turbulence Model

The Spalart – Allmaras (S-A) model is a one-equation turbulence model. As the name of their paper implies (Spalart & Allmaras, 1994), it is developed for aerodynamic flows. The model generates good results for slender bodies like airfoils or flows over flat plates where separation either does not occur or occurs very late on the body. The only equation that exists in their model solves for the turbulent viscosity in the flow which is used to take into account the velocity fluctuations in the fluid domain due to turbulence. This turbulence model is faster when compared to the other models, mostly due to containing a single equation.

The S-A model is used in various VIV papers due to its practicality. The model is used in (Wu, Bernitsas, & Maki, 2014) for smooth cylinders and also to cylinders which have partial roughness. The validation of their study was made with the experiments of (Khalak & Williamson, 1996) which have become a benchmark for computational studies in this field. They have managed to correctly represent the initial and lower branches but managed to partially get the upper branch. The turbulence model was also used to solve for tandem cylinders which had partial roughness (which is referred as "passive turbulence control or PTC in short notation" and patented by (Bernitsas & Raghavan, 2011)) in (Ding, Bernitsas, & Kim, 2013). It is stated in their paper that PTC dictates the position of the boundary layer separation and results in a good agreement between experiments and simulations.

6.2. URANS: The $k-\varepsilon$ Turbulence Model

The standard $k-\varepsilon$ model is a two-equation turbulence model which was first developed by (Jones & Launder, 1972). It is developed to solve for turbulent boundary layers which have so high accelerations that the turbulent boundary layer *laminarizes* (Jones & Launder, 1972). It is an extensively used turbulence model for solving the turbulent flow around bluff bodies. The standard $k-\varepsilon$ model was significantly improved by (Shih, William, Shabbir, Yang, & Zhu, 1995). In their study, they have stated that the realizable $k-\varepsilon$ turbulence model performs better in flows involving high shear rates or massive separations.

The $k-\varepsilon$ model is used by some researchers to solve for the highly nonlinear flow around circular cylinders. Flows around stationary cylinders and cylinders in VIV were computationally solved by (Wanderley, Souza, Sphaier, & C, 2008). They have managed to obtain a very good agreement for the stationary cylinder and for cylinder in VIV. For the cylinder in VIV, they have used the experiments of (Khalak & Williamson, 1996) and clearly captured initial, upper and lower branches using the increased

reduced velocity condition as proposed by (Guilmineau & Queutey, 2002).

6.3. URANS: The k − ω Turbulence Model

The $k-\omega$ model is a two-equation turbulence model which is used extensively for solving flows around bluff bodies. The model was improved by (Wilcox, 2008) to solve for more complicated separated flows. A more widely used version of the $k-\omega$ model is the $k-\omega SST$ model which is a hybrid method which combines the $k-\omega$ and$k-\varepsilon$ turbulence models. $k-\omega SST$uses the standard $k-\omega$ model inside the boundary layer and switches to the $k-\varepsilon$ model in the outer region (Menter, 1994).

There are many computational VIV papers using the $k-\omega SST$ turbulence model. The numerical simulations by (Pan, Cui, & Miao, 2007) reveal accurate results for the amplitude and frequency response of a cylinder subjected to VIV. However, the high amplitudes in the upper branch which are achieved experimentally by (Khalak & Williamson, 1996) were not captured in their work. This is accounted to the random disturbance of the vortex shedding being averaged in RANS. They state that the bias of amplitudes in the upper branch arise from the irregular behavior of response in the vortex formation for the cylinder in VIV. Using the same set of experiments of (Khalak & Williamson, 1996), the upper branch was partially captured by (Guilmineau & Queutey, 2002) using the increasing velocity condition.

6.4. Large Eddy Simulation (LES) and Direct Numerical Simulation (DNS)

There are more advanced methods of solving VIV computationally other than URANS methods and two of them will briefly be discussed in this section. One of the better options (but definitely more demanding in terms of computer memory) is the LES. LES dynamically adjusts the model to eliminate the small scale eddies and only solves for the large scale eddies by using two filters (Germano, Piomelli, Moin, & Cabot, 1991). It was first used by (Smagorinsky, 1963) to simulate the atmospheric air circulation.

DNS allows a direct solution of Navier-Stokes Equations without any turbulence model but is highly demanding in terms of computational power. The Kolmogorov length scale, which is used to establish the grid in the flow domain, greatly reduces as the Reynolds number of the flow increases. The Kolmogorov length scale is inversely proportional to the number of mesh elements on a body. Increasing the Reynolds number results in a higher number of elements needed to solve for the flow (Landahl & Mollo-Christensen, 1992). Due to this reason, DNS is usually applied to flows which have very low Reynolds numbers.

URANS generally provides a good understanding of the flow in terms of quantitative data like the lift force or the amplitude. However, it is stated by (Sarpkaya, 2004) that a greater understanding about the wake – boundary layer interaction will be achieved by simulating VIV with LES and DNS. 2D and 3D simulations of VIV were made by (Tutar & Holdo, 2000) to investigate the vortex structure formed behind a smooth circular cylinder at $Re = 24000$. A hybrid RANS-LES method named as Detached Eddy Simulation (DES) was used to solve for 3D simulation of VIV of a circular cylinder by (Saltara, D'Agostini Neto, & Lopez, 2011)at $Re = 10000$. High amplitudes occurring at the upper branch were captured in their simulations. The correlation length in the near wake was investigated by (Lucor, Foo, & Karniadakis, 2003) with DNS at $Re = 3000$. A computational study at $Re = 10000$, which is the highest Reynolds number achieved in the open literature using DNS, was made by (Dong & Karniadakis, 2005). They have presented their results for stationary and oscillating cylinders and found good agreement with the experiments.

6.5. Comparison of URANS Turbulence Models with a Benchmark Case

The CFD results of the amplitude response of the cylinder from the literature are given in Fig. 3 using URANS turbulence models. All results are produced with the commercial CFD code, ANSYS Fluent, and compared with the benchmark experimental results of (Khalak & Williamson, 1996). In this figure, only the results for which the cylinder starts from rest are shown. The results of the present study implementing the $k-\omega SST$ turbulence model are also included in the figure. In that figure, U^* is calculated as:

$$U^* = \frac{U_{fs}}{f_{n,a} \cdot D} \tag{14}$$

where$f_{n,a}$ is calculated as:

$$f_{n,a} = \frac{1}{2\pi}\sqrt{\frac{k}{m}} \tag{15}$$

Although Khalak and Williamson's experiments were conducted in water, they have non-dimensionalized the reduced velocity, U^* with the natural frequency in air, $f_{n,a}$. Their experiments were conducted starting from$Re = 3800$. Due to the selected turbulence model, the maximum $y+$ value on the cylinder surface is around 10 (ANSYS Fluent 12 User's Guide, 2009).

Figure 3 is a proof of the existence of many computational approaches that could be made. The selection of the turbulence model is not the only criteria that vary the results. Some other parameters like the grid structure, the implementation of the dynamic mesh, the numerical algorithm and the selection of the time step size also play a role in the results obtained. Although the same turbulence model is used by (Guilmineau & Queutey, 2002), (Pan, Cui, & Miao, 2007) and the present study, the amplitude response of the cylinder in each reduced velocity differs.

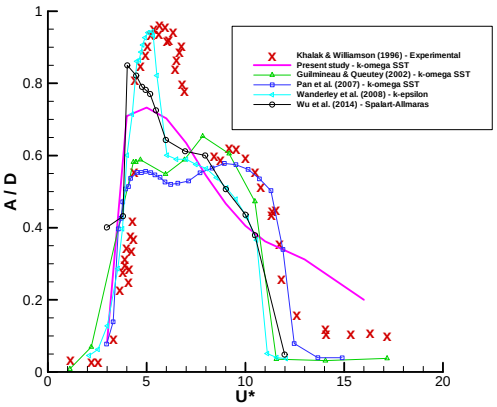

Fig. 3. Comparison of CFD results implementing URANS with the experimental results of (Khalak & Williamson, 1996).

The closest computational results to the experiments are obtained by (Wanderley, Souza, Sphaier, & C, 2008) with the $k-\varepsilon$ model. They have used the Roe-Sweby scheme to numerically solve the slightly compressible RANS equations in combination with the $k-\varepsilon$ turbulence model. They state that these three have combined to return accurate results.

7. CALCULATION OF TIME STEP SIZE

Time step size is determined by the CFL (Courant-Friedrichs-Lewy) condition which is given as:

$$\frac{u \cdot \Delta t}{\Delta x} \leq C_{max} \tag{14}$$

where C_{max} is selected to be equal to one due to the utilization of an explicit solver. As dictated by Eq. 17, the time step size is sensitive to the element size close to the cylinder. As the element size decreases, the time step size decreases proportionally which increases the computation time significantly for solvers implementing LES and (especially) DNS methods.

8. NUMERICAL RESULTS FOR VIV IN TrSL3 FLOW REGIME

The results presented in Section 6 have $Re = 3800$ and is in the TrSL2 regime (Zdravkovich, 2003). However, the approach used in this study is robust and can handle flows forhigher Re. The results of (Park, Bernitsas, & Kumar, 2012) are used here to compare CFD approach with experiments.

The oscillator system particulars are given in Table 1. The added mass of the cylinder is taken as the added mass in still water, which is equal to one, to be in accordance with the reference study. During the experiments, the spring stiffness was kept constant while the fluid velocity was changed to adjust the reduced velocity, U^*. The Reynolds number range was between $35{,}000 < Re < 130{,}000$. For moredetails on the conducted experiments, please refer to (Park, Bernitsas, &Kumar, 2012).

Table 1 Oscillator system particulars

Mass of the oscillating system	m_{osc}	kg	9.784
Displaced fluid mass	m_d	kg	5.6707
Added mass	m_a	kg	5.6707
Mass ratio	m^*	kg	1.725
Natural frequency in still water	$f_{n.w}$	Hz	1.1183
Damping ratio	ζ	$-$	0.0158

The amplitude and frequency responses of the cylinder are given in Figs. 4 and 5. In Fig. 5, the oscillation frequency f_{osc} is non-dimensionalized by the natural frequency in still water $f_{n.w}$, given as:

$$f^* = \frac{f_{osc}}{f_{n,w}} \tag{15}$$

where the $f_{n,w}$ is calculated by,

$$f_{n,w} = \frac{1}{2\pi}\sqrt{\frac{k}{m+m_a}} \tag{16}$$

The different branches in the amplitude response of the cylinder are clearly visible in Fig. 4. The initial branch is between $5 < U^* < 6$ in the experiments while it occurs before that in the CFD, which is between $4 < U^* < 5$. The results of the numerical approach suggest that the upper branch occurs between $5 \leq U^* \leq 10$. Looking at the amplitude response, it may be said that the range of synchronization is captured very well with CFD, as the end of the synchronization is also at $U^* = 10$ in the experiments. On the other hand, CFD cannot capture the maximum amplitude achieved by the cylinder in experiments. This is accounted to the simplifications in the turbulence models that URANS uses. Random behavior of the flow and its chaotic character plays an important role in getting the high amplitudes in the upper branch but URANS averages these random behaviors of the flow; restricting the maximum achieved amplitude. Both the results of the CFD and the experiments show that the oscillating cylinder goes into de-synchronization with the flow after $U^* > 10$.

The time versus force and displacement at $U^* = 5$ was investigated to find out if the cylinder is in synchronization with the fluid force. This is given in Fig. 6.The value of $U^* = 5$ was specifically chosen because it is the equivalent of $St = 0.2$, which is approximately the vortex shedding frequency of a stationary cylinder. It was found out that although the CFD approach can point out the synchronization of the fluid force with the cylinder oscillation in the upper branch, it fails to grasp the maximum amplitude achieved. A possible reason for this might be that the CFD approach cannot capture the strength of the vortex mechanism in the upper branch. So the fluid force F in Eq. (1) is calculated to be less than what is actually exerted on the cylinder. It is considered that lower Fresults in

lower amplitudes and creates the bias of results between calculations and experiments.

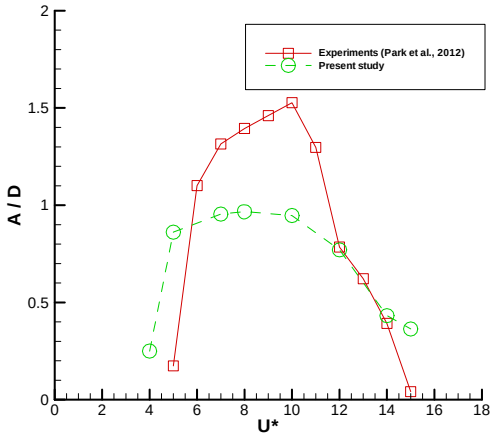

Fig. 4. Amplitude response of the cylinder with URANS compared to the experiments of (Park, Bernitsas, & Kumar, 2012).

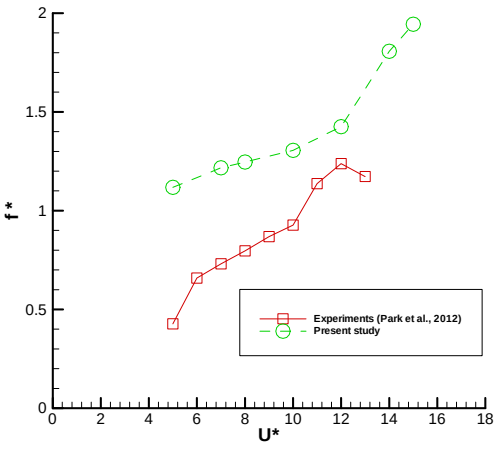

Fig. 5. Frequency response of the cylinder with URANS compared to the experiments of (Park, Bernitsas, & Kumar, 2012).

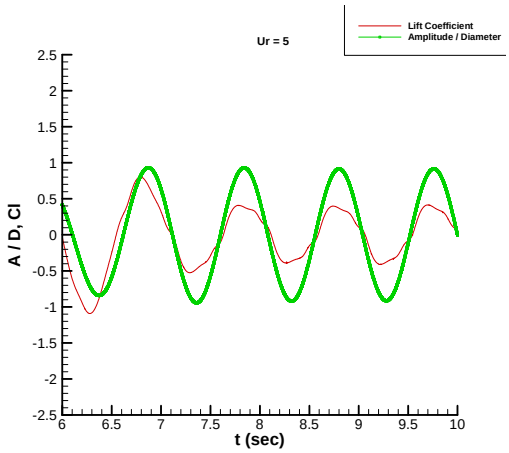

Fig. 6. Time versus fluid force and displacement in the upper branch at $U^* = 5$.

9. CONCLUSION

This study reveals a CFD based approach to solve for vortex-induced vibrations of circular cylinder. The approach is first validated by a benchmark low Reynolds number, experimental study and then the results are extended to higher Reynolds numbers. It is found out that the approach implemented in this study returns satisfactory results for the TrSL2 flow regime. For flows between $35{,}000 < Re < 130{,}000$, the distinction between different branches can be noticed from CFD results and the range of synchronization is correctly captured. However, the maximum amplitude achieved by the cylinder in the upper branch was not captured with CFD and this problem is also mentioned by some other researchers in the field (Guilmineau & Queutey, 2002), (Pan, Cui, & Miao, 2007). URANS can return accurate and fast results quantitatively for practical purposes but due to the insufficiency of the method, the wake modes and the physics of the flow should be investigated by more advanced methods like LES and DNS as also proposed by (Sarpkaya, 2004).

ACKNOWLEDGMENTS

The financial support of The Scientific and Technological Research Council of Turkey (TUBITAK) is gratefully acknowledged.

REFERENCES

ANSYS Fluent 12 User's Guide. (2009, April).

Bernitsas, M. and K.Raghavan (2011). *Patent No. 8,042,232 B2.* USA.

Ding, L., M.Bernitsas and E.Kim (2013). 2-D URANS vs. experiments of flow induced motions of two circular cylinders in tandem with passive turbulence control for 30,000<Re<105,000. *Ocean Engineering*, 429-440.

Dong, S. and G.Karniadakis (2005). DNS of flow past a stationary and oscillating cylinder at Re=10000. *Journal of Fluids and Structures*, 519-531.

Germano, M., U.Piomelli, P.Moinand W.Cabot (1991). A dynamic subgrid-scale eddy viscosity model. *Physics of Fluids*, 1760-1765.

Guilmineau, E.and P.Queutey (2002). A numerical simulation of vortex shedding from an oscillating circular cylinder. *Journal of Fluids and Structures*, 773-794.

Jones, W. and B.Launder (1972). The prediction of laminarization with a two-equation model of turbulence. *International Journal of Heat and Mass Transfer*301-314.

Khalak, A. and C.Williamson (1996). Dynamics of a hydroelastic cylinder with very low mass and damping. *Journal of Fluids and Structures*, 455-472.

Landahl, M. and E. Mollo-Christensen (1992). *Turbulence and random processes in fluid mechanics (2nd ed.).* Cambridge University Press.

Lucor, D., J. Foo and G.Karniadakis (2003). Correlation length and force phasing of a rigid cylinder subject to VIV. *IUTAM Symposium on Fluid-Structure Interactions.* USA: Rutgers State University.

Menter, F. (1994). Two-equation eddy-viscosity turbulence models for engineering applications. *AIAA Journal*, 1598-1605.

Pan, Z., W. Cui and Q. Miao (2007). Numerical simulation of vortex-induced vibration of a circular cylinder at low mass-damping using RANS code. *Journal of Fluids and Structures*, 23-37.

Park, H., M. M. Bernitsas and R. A. Kumar (2012). Selective roughness in the boundary layer to suppress flow-induced motions of circular cylinders at 30,000<Re<120,000. *Journal of Offshore Mechanics and Arctic Engineering* , 041801.

Raghavan, K., M. M. Bernitsas and D. E.Maroulis (2009). Effect of bottom boundary on VIV for energy harnessing at 8x10^3<Re<1.5x10^5. *Journal of Offshore Mechanics and Arctic Engineering*, 031102.

Saltara, F., A. D'Agostini Neto and J.Lopez (2011). 3D CFD simulation of vortex-induced vibration of cylinder. *International Journal of Offshore and Polar Engineering*, 192-197.

Sarpkaya, T. (2004). A critical review of the intrinsic nature of vortex-induced vibrations. *Journal of Fluids and Structures*, 389-447.

Shih, T., W. William, A. Shabbir, Z. Yang and J. Zhu (1995). A new k-ε eddy viscosity model for high Reynolds number turbulent flows. *Computers* and *Fluids*, 227-238.

Smagorinsky, J. (1963). General circulation experiments with the primitive equations, I. the basic experiment. *Monthly weather review*, 99-164.

Spalart, P. and S. Allmaras (1994). A one-equation turbulence model for aerodynamic flows. *Recherche Aerospatiale*, 5-21.

Tutar, M. and A. Holdo (2000). Large eddy simulation of a smooth circular cylinder oscillating normal to a uniform flow. *ASME Journal of Fluids Engineering*, 694-702.

Wanderley, B., G. Souza andC. L. S. Sphaier(2008). Vortex-induced vibration of an elastically mounted circular cylinder usig an upwind TVD two-dimensional numerical scheme. *Ocean Engineering*, 1533-1544.

Wilcox, D. (2008). Formulation of the k-ω turbulence model revisited. *AIAA Journal*, 2823-2838.

Willimson, C. and R.Govardhan (2004). Vortex-Induced Vibrations. *Annual Review of Fluid Mechanics*, 413-455.

Wu, W., M. Bernitsas and K.Maki (2014). RANS simulation versus experiments of flow induced motion of circular cylinder with passive turbulence control at 35,000<Re<130,000. *Journal of Offhsore Mechanics and Arctic Engineering*, 041802-1-041802-10.

Zdravkovich, M. M. (2003). *Flow Around Circular Cylinders.* New York: Oxford University Press.